Optimization Design of Halbach Permanent Magnet Motor Based on Multi-objective Sensitivity

Shuangshuang Zhang, Wei Zhang, *Member, IEEE,* Rui Wang,
Xu Zhang, and Xiaotong Zhang

***Abstract*—The halbach permanent magnet synchronous motor (HPMSM) combines the advantages of permanent magnet motors and halbach arrays, which make it very suitable to act as a robot joint motor, and it can also be used in other fields, such as electric vehicles, wind power generation, etc. At first, the sizing equation is derived and the initial design dimensions are calculated for the HPMSM with the rated power of 275W, based on which the finite element parametric model of the motor is built up and the key structural parameters that affect the total harmonic distortion of air-gap flux density and output torque are determined by analyzing multi-objective sensitivity. Then the structure parameters are optimized by using the cuckoo search algorithm. Last, in view of the problem of local overheating of the motor, an improved stator slot structure is proposed and researched. Under the condition of the same outer dimensions, the electromagnetic performance of the HPMSM before and after the improvement are analyzed and compared by the finite element method. It is found that the improved HPMSM can obtain better performances.**

***Index Terms*—Halbach permanent magnet synchronous motor, multi-objective sensitivity, cuckoo search algorithm, electromagnetic characteristics, finite element analysis.**

I. Introduction

JOINT robots not only can replace manpower to complete work in harsh environments such as high temperature, radiation, and corrosion, but also can be used to improve production efficiency, shorten production cycles, and reduce labor intensity in product production [1]. It has an irreplaceable position in the transformation and upgrading of traditional manufacturing industries [2].The motor is one of the most important parts of the robot because it is essential for the smooth, accurate, and reliable operation of the robot. The main joint motors currently used in robots include stepping motor, direct current motor, and permanent magnet motor [3]-[7].

The permanent magnet motor has become a research hot spot in joint motors because of its small size, wide speed range, and large starting torque. In order to further satisfy the requirements for low-mass, high-torque joint motors of biological robots, the different topologies have been researched in recent years. Axial flux permanent magnet machine with high torque density was proposed and compared with radial flux BLDC motor in [8] and [9]. It was found that the axial field permanent magnet machine could provide larger output torque than radial flux BLDC motor. However, the torque ripple was not able to be ignored due to the large cogging torque. W. Zhang studied a permanent magnet motor with fractional slot concentrated winding [10]. Although the torque was largely improved, it also brought the problems of low efficiency and large loss. In 1980, Dr. Klaus Halbach first proposed halbach permanent magnet array [11]. The halbach array is made by inserting permanent magnets with different magnetization directions according to a certain law. It forms a self-shielding effect [12]. Appling the halbach array into the permanent magnet synchronous motor and optimizing the structural parameters of the motor, the output torque can be increased [13]. In addition, the torque ripple and losses can be reduced. These are beneficial to the application of joint motors.

At present, there are many optimization methods were used for permanent magnet motors, such as hybrid genetic-simulated annealing algorithm, fuzzy-based Taguchi method, hybrid multi-objective optimization algorithm and so on. In [14], the fuzzy-based Taguchi method was applied to the multi-objective optimization of direct-driven permanent magnet synchronous motor，by which solved the problem that the fuzzy algorithm was limited by the number of objective functions. However, it had a slow convergence rate. A hybrid multi-objective optimization algorithm had a fast convergence rate, but the global search ability was poor [15]. In [16] and [17], the multi-objective analysis was carried out to optimize the motor by applying a hybrid genetic-simulated annealing algorithm and conformal mapping method, respectively. By which the performance of the machine could be improved, but both methods were prone to premature stagnation. In order to improve the magnetic density of halbach array and reduce harmonic contents, the genetic algorithm was used to optimize halbach array with unequal thickness [18]. It was found if there

Manuscript was submitted for review on 29, January, 2020.

This work was supported by the National Natural Science Foundation of China (51507087), the Six Talents Summit Project of Jiangsu Province (XNYQC-017) and the Science and Technology Planning Project of Nantong City (MS22019017).

Shuangshuang Zhang is with the School of Electrical Engineering, Nantong University, Nantong, 226019, China (e-mail: 17551314976@163.com).

Wei Zhang is with the School of Electrical Engineering, Nantong University, Nantong, 226019, China (e-mail: zhang.w@ntu.edu.cn). She is the corresponding author.

Rui Wang is with the School of Electrical Engineering, Nantong University, Nantong, 226019, China (e-mail: 908848262@qq.com).

Xu Zhang is with the School of Electrical Engineering, Nantong University, Nantong, 226019, China (e-mail: zhangxu_ele@126.com).

Xiaotong Zhang is with the School of Electrical Engineering, Nantong University, Nantong, 226019, China (e-mail: 892360579@qq.com).

Digital Object Identifier 10.30941/CESTEMS.2020.00004

were many parameters for multi-objective optimization, the ability of this algorithm to quickly optimize would be weakened. The Non-dominated Sorting Genetic Algorithm technique was used to optimize the efficiency, size and mass of a permanent-magnet generator in which could arbitrarily select the number of optimization goals by non-dominated set ordering [19]. However, it increased the complexity and amount of calculation. Based on a Tabu search algorithm and finite element method, permanent magnet motor with halbach magnets was optimized [20]. Although this algorithm overcame the shortcomings of genetic and simulated annealing algorithm, which were prone to mature prematurely, it relied heavily on the initial design values. Poor initial values may result in the bad optimization results.

According to the above mentioned, in some extent, the optimization results of permanent magnet motors can be improved by the intelligent algorithms. However, there are still empirical limitations in the choice of initial design variables. It can lead to time-consuming and inefficient optimization design. Therefore, the key structural parameters that have the greatest impact on optimal goals are quickly chosen for halbach permanent magnet synchronous motors (HPMSM) based on multi-objective sensitivity in this paper.

The basic principle of HPMSM is described in Section II, and initial design parameters of HPMSM are determined. In Section III, the HPMSM is optimized and improved by multi-objective sensitivity and cuckoo search algorithm (CSA). The experiments are done for the improved HPMSM in Section VI. The conclusion is given in Section V.

II. Basic Principle and Initial Design of HPMSM

A. Basic Structure of HPMSM

Fig. 1 shows the 3D topology of three-phase HPMSM, which composed of stator and rotor iron cores, armature windings and 20 groups of halbach arrays. The materials of the stator and rotor iron core are silicon steel sheets, 100 blocks of NdFeB comprise halbach arrays, and the armature windings are made up of copper coils.

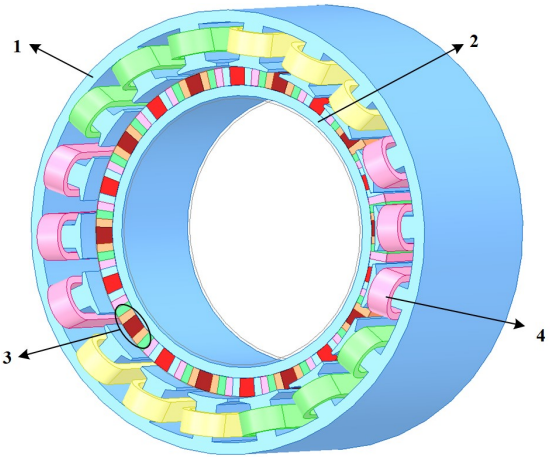

Fig. 1. Three-dimensional topology of HPMSM.
1-stator, 2-rotor, 3-permanent magnets, 4-winding.

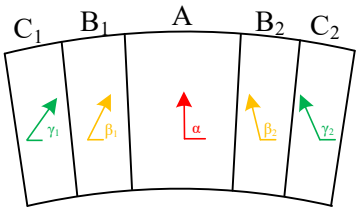

Fig. 2. Magnetization angles of each halbach array.

In Fig.2, each halbach array consists of five permanent magnets with different magnetization directions labeled as A, B_1, B_2, C_1, and C_2, respectively, and those magnetization angles are α, β_1, β_2, γ_1, and γ_2, respectively, and defined as (1).

$$\begin{aligned} &\alpha=\pi+k\cdot 18\left(k=0,1,2\cdots 19\right)\\ &\beta_1=\pi-\beta_2\\ &\gamma_1=\pi-\gamma_2 \end{aligned} \tag{1}$$

where k is the rotation offset coefficient.

B. Original Design of HPMSM

The output power P_2, the induced electromotive force E_m and the permanent magnetic flux Φ_m are shown in (2) ~ (4), respectively.

$$P_2=\eta P_1=\eta m E_m I_m \tag{2}$$

$$E_m=N_{ph}\omega_r 2p\Phi_m \tag{3}$$

$$\Phi_m=k_d k_F B_{g\max} C_s \frac{1}{P_s}\frac{\pi}{4}\left(D_{so}^2-D_{si}^2\right) \tag{4}$$

where m is the number of phases, , I_m is the magnitude of the stator phase current, η is the efficiency, N_{ph} is the turn number of the stator phase windings, ω_r is the angular velocity of the rotor, k_d is the winding factor, k_F is the waveform factor of the air-gap flux, $B_{g\,max}$ is the maximum value of the air-gap flux density, C_s is the calculating pole-arc coefficient, P_s is the number of stator slots, D_{si} and D_{so} are the inner and outer diameter of the stator, respectively.

Substituting (4) into (3), (5) can be derived.

$$E_m=N_{ph}\omega_r 2Pk_d k_F B_{g\max} C_s \frac{1}{P_s}\frac{\pi}{4}(D_{so}^2-D_{si}^2) \tag{5}$$

The armature current amplitude I_m is given by (6).

$$I_m=\sqrt{2}I_{ms}=\sqrt{2}\frac{A_s\pi D_{si}}{mN_{ph}} \tag{6}$$

where A_s is the line load of the winding inner diameter, I_{ms} is the effective value of the armature winding phase current.

Substituting (5) and (6) into (1), (7) is derived.

$$P_2=\frac{\sqrt{2}\pi^3}{60}\frac{p}{P_s}k_d k_F D_{si}(D_{so}^2-D_{si}^2)A_s B_{g\max} C_s n\eta \tag{7}$$

(8) is derived from (7).

$$D_{so}^3=\frac{P_2}{\frac{\sqrt{2}p}{60P_s}\pi^3 k_d k_F k_{io}(1-k_{io}^2)A_s B_{g\max} C_s n\eta} \tag{8}$$

where k_{io} is split ratio of HPMSM, $k_{io}=D_{si}/D_{so}$.

The initial design parameters are calculated by (8) and as shown in Table I, according to the performance indexes

demands of the rated power P_2 =275W, the rated speed n_N = 2100 r/min, the rated voltage U_N = 48V, and η=89%. The geometric parameters of HPMSM are depicted in Fig.3.

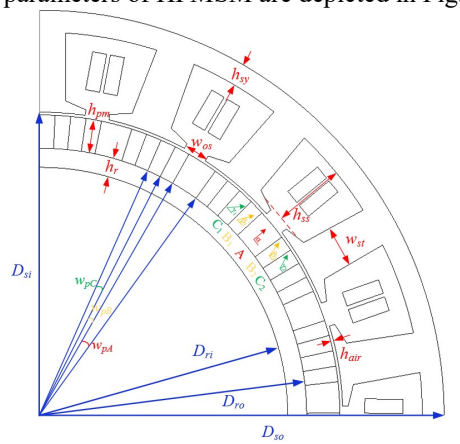

Fig. 3. The geometric parameters of HPMSM.

TABLE I
THE INITIAL DIMENSIONS OF HPMSM

Symbol/Unit	Title	Value
D_{si}/mm	Inner diameter of stator	21.1
D_{so}/mm	Outer diameter of stator	25
D_{ri}/mm	Inner diameter of rotor	15
D_{ro}/mm	Outer diameter of rotor	19.5
l/mm	Axial length of stack	20.7
h_{pm}/mm	Height of permanent magnet	1.4
w_{pA}/ (°)	Thickness of permanent magnet A	6
α/ (°)	Magnetization direction of A	90
w_{pB}/ (°)	Thickness of magnet B_1	3
β/ (°)	Magnetization direction of B_1	30
w_{pC}/ (°)	Thickness of permanent magnet C_1	3
γ/ (°)	Magnetization direction of C_1	45
w_{st}/ (°)	Width of stator tooth	5.4
h_{ss}/mm	Height of stator slot	2.4
h_{sy}/mm	Height of stator yoke	1
w_{os}/ (°)	Width of stator slot	7
h_{air}/mm	Height of air gap	0.2

III. OPTIMIZATION AND STRUCTURAL IMPROVEMENT OF HPMSM

The optimal design flow chart of HPMSM is shown in Fig. 4. In this paper, the initial parameters are designed for HPMSM with the rated power of 275W by (2) ~ (8). Then a parametric model of HPMSM is established to evaluate the electromagnetic performance of the motor. Due to the huge workload of the traditional single parameter optimization method, the multi-objective sensitivity method is used to obtain the key structural parameters，based on which the CSA is used to optimize the structural parameters of HPMSM，so that the efficiency and accuracy of the optimization design of HPMSM are both improved.

A. Multi-objective Sensitivity Analysis of HPMSM

In order to obtain the large torque and small torque ripple of HPMSM, the total harmonic distortion of air-gap flux density (THD_{Br}) and output torque are chosen to be two optimal goals.

By the sensitivity analysis, the parameters that have the greater impact on the optimization targets of HPMSM can be determined. According to the constraints of actual manufacture

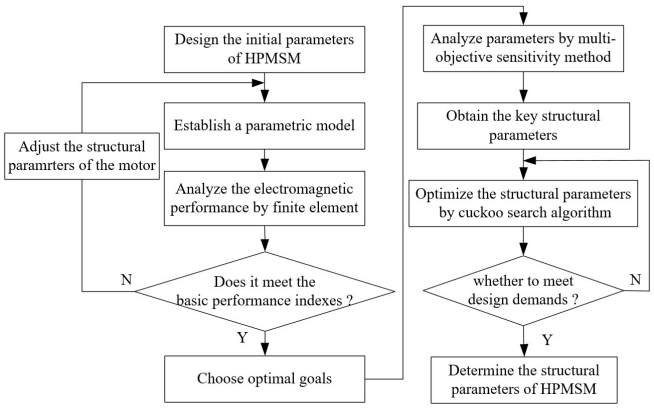

Fig. 4. Flow chart of optimal design of HPMSM.

condition, among the multiple structural parameters in Table I, the eight structural parameters of the HPMSM are selected as design variables to analyze multi-objective sensitivity. The variables and their optimization ranges are shown in Table II.

TABLE II
OPTIMIZATION RANGE OF KEY PARAMETER VARIABLES

Symbol/Unit	Title	Range
β/ (°)	Magnetization direction of B_1	20 ~ 30
γ/ (°)	Magnetization direction of C_1	32 ~ 48
w_{st}/ (°)	Width of stator tooth	4.32 ~ 6.48
h_{sy}/mm	Height of stator yoke	1.2 ~ 1.8
h_{ss}/mm	Height of stator slot	1.28 ~1.92
w_{os}/ (°)	Width of stator slot	5.6 ~ 8.4
h_{pm}/mm	Height of permanent magnet	1 ~ 3
h_r/mm	Height of rotor yoke	3.6 ~ 5.4

According to (9), the sensitivity of different main structural parameters $S(X)$ are calculated, and the analysis results are shown in Fig.5.

$$S(X) = Avg[S(Xi)] = Avg\left\{\frac{\left\{\frac{F(X_0 \pm \Delta Xi) - F(X_0)}{F(X_0)}\right\}}{\left\{\frac{\pm\Delta(Xi)}{X_0}\right\}}\right\} \tag{9}$$

where X is the design parameter variable, X_0 is the initial value of X, and X_i is defined as 10%, 15%, and 20% of its initial value, respectively. $S(X_i)$ is the sensitivity index of X_i, $AvgS(X_i)$ is the average value of $S(X_i)$, $F(X_0)$ is the value of optimization objective under the condition of X_0.

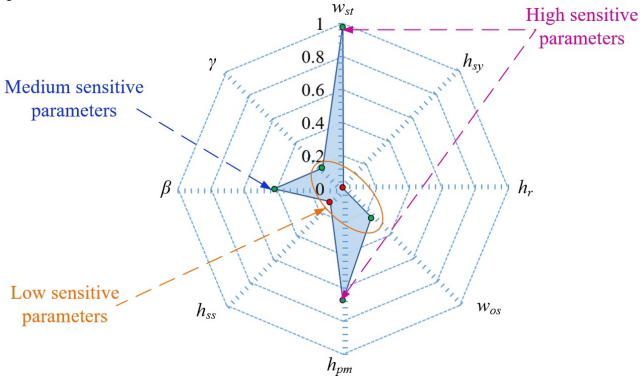

(a) Total harmonic distortion of air-gap flux density.

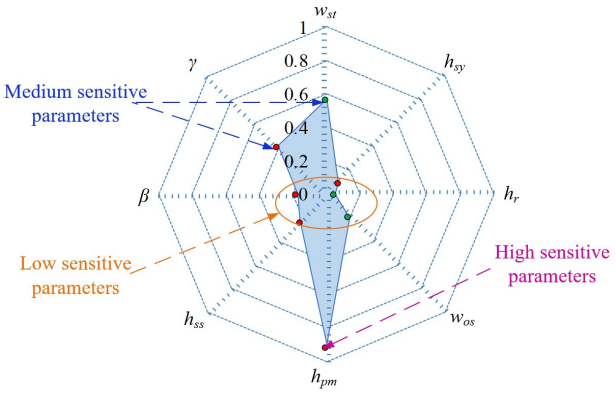

(b) Output torque.

Fig. 5. Multi-objective sensitivity analysis.

Fig.5 demonstrates the sensitivity analysis of the THD_{Br} and output torque under the condition of the different design variables, in which the red dot represents positive data of sensitivity, and the green dot is negative data. If the sensitivity is far away from the center of the circle, the parameter is the more sensitive.

The sensitivity less than 0.4 is defined as low sensitive parameters. The sensitivity greater than 0.6 is defined as high sensitive parameters. The sensitivity between 0.4 and 0.6 is defined as medium sensitive parameters.

It can be seen from Fig.5 (a) that w_{st}, h_{pm} are high sensitivity parameters for THD_{Br}. In addition, γ, h_{ss}, w_{os} and h_{sy} are low sensitive parameters, β is medium sensitive parameters for THD_{Br}.

Similarly, h_{pm} is high sensitive parameters for the output torque that can be quickly found from Fig.5 (b). Meanwhile, β, h_{ss}, w_{os} and h_{sy} are low sensitive parameters, w_{st} and γ are medium sensitive parameters for the output torque.

Therefore, through parameter sensitivity analysis, the crucial variables that have greater impacts on the optimization targets are determined intuitively and quickly, which is beneficial to reduce time consumption and improve efficiency of the multi-objective optimization.

B. *Optimization Based on CAS*

According to Fig.5, the w_{st}, h_{pm} are chosen as key sensitivity parameters and they are optimized by CSA. First, the two optimal targets are fitted by the surface response method, and the function expressions of the output torque and the THD_{Br} are obtained, as shown in (10) and (11) , respectively.

$$f_T = 0.028w_{st}^2 - 0.017h_{pm}^2 + 0.012w_{st}h_{pm} + 0.061w_{st} + 0.223h_{pm} - 0.041 \quad (10)$$

$$f_{THD_{Br}} = 1.32w_{st}^2 + 1.68h_{pm}^2 + 2.99w_{st}h_{pm} - 13.14w_{st} - 13.97h_{pm} + 47.93 \quad (11)$$

In addition, the Pareto optimal solution sets of the objective functions are obtained by the CSA, as shown in Fig.6.

Because the output torque and the THD_{Br} are of equal importance to the performance of HPMSM, the optimal solution is chosen and labeled in Fig.6 and the optimal values are shown in Table III. It is found from TABLE III that the proposed optimal method can obtain the optimal parameters quickly and efficiently.

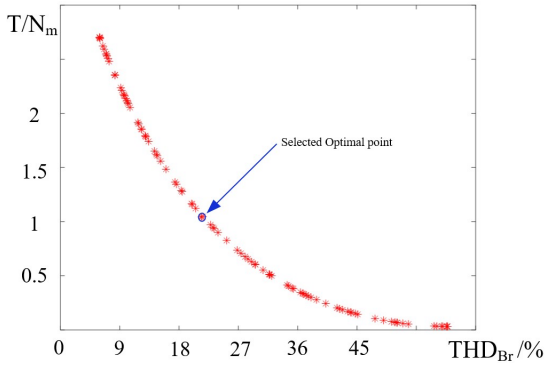

Fig. 6. Pareto optimal solution sets.

TABLE III
COMPARISON OF BEFORE AND AFTER OPTIMIZATION

Parameters/Unit	Value	
	Before optimization	After optimization
w_{st} / (°)	5.4	5
h_{pm} /mm	1.4	2.9
Output torque /Nm	0.98	1.12
THD_{Br} /%	23.7	19.5
P_2 /W	275	284
η /%	89	90.4

C. *Air-gap* flux *Density Cloud Map of HPMSM*

Fig.7 is the air-gap flux density cloud map of the after optimization of HPMSM. It can be found that the stator teeth have local magnetic saturation, which could cause the problem of motor overheating, so that the risk of motor burnout and permanent magnet demagnetization may be both increased.

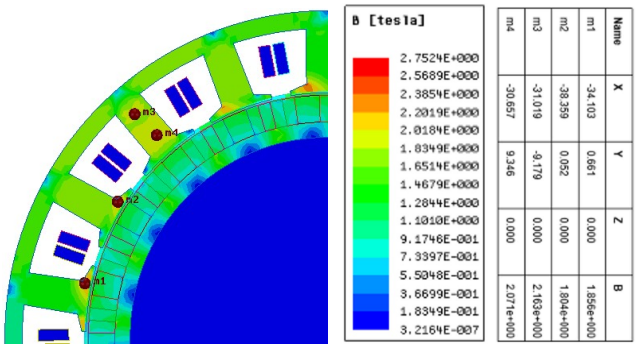

Fig. 7. Magnetic flux density map of after optimization.

D. *Improved structure of HPMSM*

In view of the above problems, the stator slot of the HPMSM is improved without changing the other structures of HPMSM. The improved stator slot structure is shown in Fig.8. For the convenience of description, the HPMSM before improvement is indicated by $HPMSM_1$, and the improved HPMSM is indicated by $HPMSM_2$.

As shown Fig.8, the stator slot is divided into an upper slot and a lower slot by a slot wedge in the radial direction. The upper slot has a fan-shaped structure in the radial section, and the lower slot has a circular wine glass-shaped structure in the radial section.

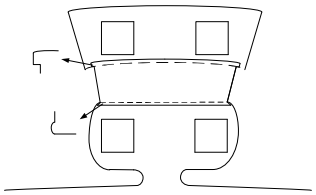

Fig. 8. Structure of improved stator slot.

E. Air-gap flux density cloud map of HPMSM2

Fig.9 is the air-gap flux density cloud map of $HPMSM_2$. By comparing Fig.7 and Fig.9, it can be seen that the local teeth magnetic density of the $HPMSM_1$ is as high as 2.163T while the local teeth magnetic density of $HPMSM_2$ is reduced by about 9.1%, the over saturation point is significantly reduced and the local overheating problem of the motor is effectively solved.

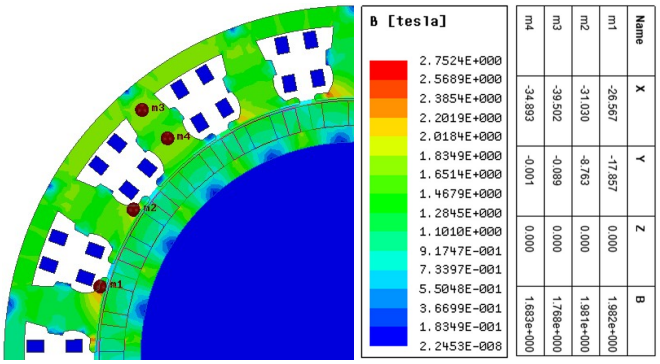

Fig. 9. Magnetic flux density map of improved motor.

F. Air-gap Flux Density

Fig.10 and Fig.11 show the flux density distribution and the harmonic analysis of air-gap flux density of $HPMSM_1$ and $HPMSM_2$, respectively. It can be seen from Fig.10 that the flux density amplitude of $HPMSM_2$ is larger than that of $HPMSM_1$, and the THD_{Br} of $HPMSM_1$ is 19.5%, while the THD_{Br} of $HPMSM_2$ is reduced by 6.1%. Thus, the fundamental amplitude of the air gap flux density of the improved HPMSM is increased. Those are beneficial to reduce torque ripple and losses, and improve output torque.

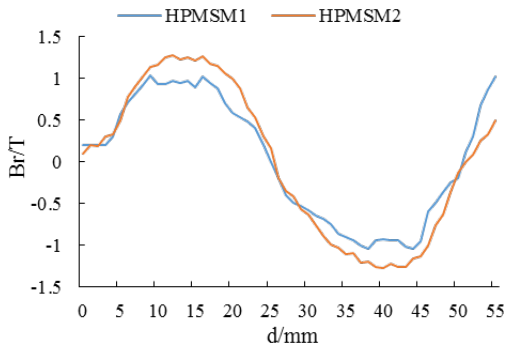

Fig. 10. Flux density distribution of air-gap magnetic field.

G. No-load Back EMF

Fig.12 shows the comparison of no-load back EMF of $HPMSM_1$ and $HPMSM_2$. When the two machines operate at the speed of 2100 r/min, the total harmonic distortion rates of the no-load back EMF waveforms are both less than 5%. In Fig. 12, the effective value of no-load back EMF of $HPMSM_2$ is 16.5 V,

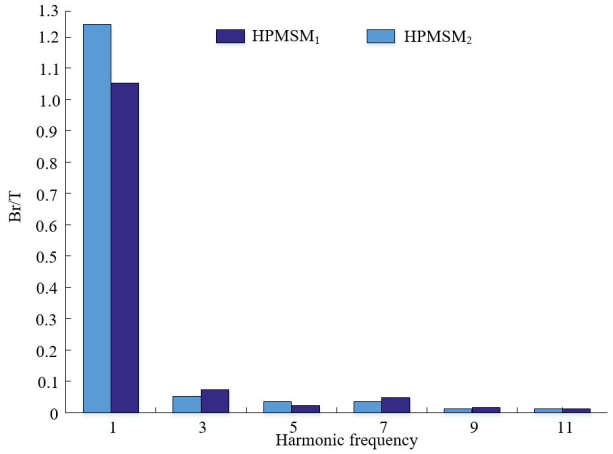

Fig. 11. Harmonic analysis of air-gap flux density.

and it is increased by 17.9% than that of $HPMSM_1$.

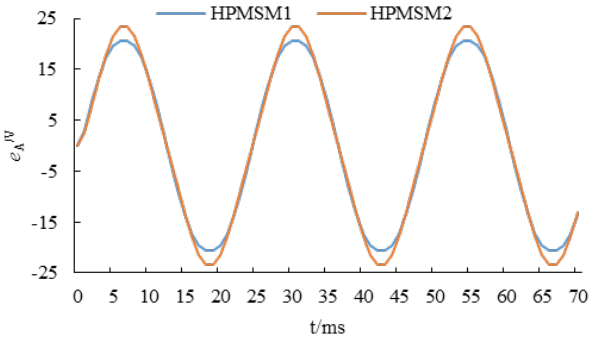

Fig. 12. Comparison of no-load back EMF.

H. Torque Characteristics

The 48V DC power supply is as input source to drive the both motors respectively. As shown in Fig. 13, the output torque of the $HPMSM_2$ is 1.25 Nm, which is 25% higher than $HPMSM_1$. And the torque ripple of $HPMSM_2$ is 4.8%, which is 1.7% less than that of $HPMSM_1$. It can be seen from Fig.13 that the torque characteristic of $HPMSM_2$ is significantly improved in contrast with HPMSM1. The torque ripple is calculated by (12).

$$k_{ripple} = \frac{T_{out(\max)} - T_{out(\min)}}{T_{out(avg)}} \times 100\% \tag{12}$$

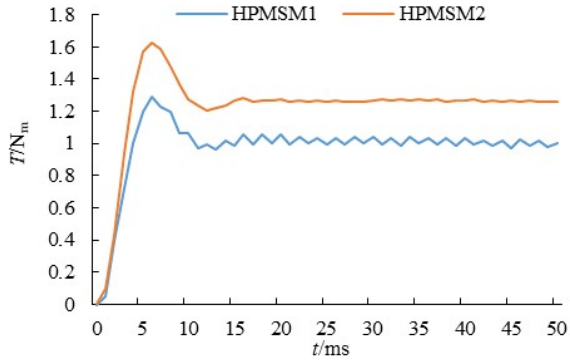

Fig. 13. Comparison of output torque.

IV. Experimental Validation

The allocation diagram of the prototype is shown in Fig. 14.

In order to verify the proposed design method, the experimental platform is built, as shown in Fig. 15. The experimental platform consists of oscilloscope, performance tester, PC, DC power supply, driver, hysteresis dynamometer and HPMSM.

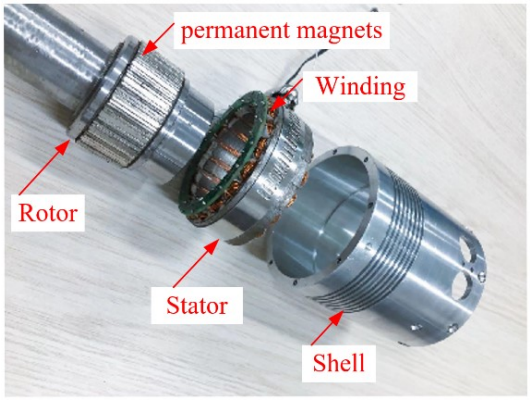

Fig.14. Allocation diagram of HPMSM prototype.

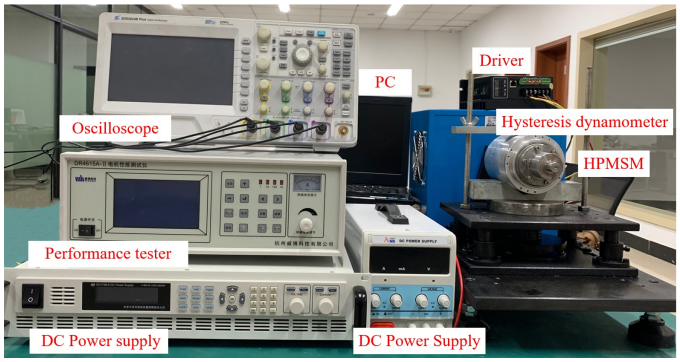

Fig. 15. Experimental platform.

When the HPMSM operates at 2100 r/min, the waveform of the measured no-load back-EMF is shown in Fig. 16. It can be seen that the back-EMF waveform is sinusoidal and symmetrical, and the amplitude of voltage reaches 22.9V. It is found that the amplitude value of the back-EMF in Fig.12 is 23.3V, which is similar to the experiment value.

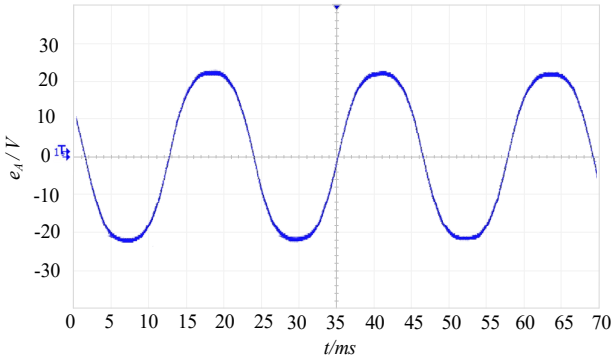

Fig. 16. No-load back-EMF waveform.

In Fig.17, the measured output torque of the HPMSM is got by the hysteresis dynamometer. It can be observed that the motor torque reaches 1.247 Nm at rated load. Meanwhile, the torque ripple is about 8.66% which is larger than that of the simulation result in Fig.13, because of the accuracy of manufacture and measure error.

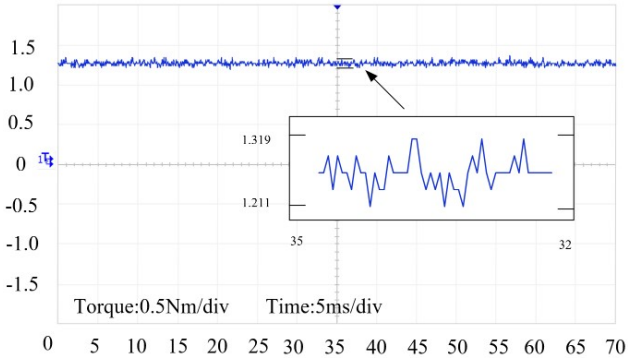

Fig. 17 Output torque at rated speed.

V. Conclusion

Among the many structural parameters of HPMSM, the sensitivity parameters that have the greatest impact on HPMSM air-gap flux density and torque are selected by multi-objective sensitivity analysis. And combined with the CSA, the optimal structure parameters of the HPMSM are quickly and efficiently determined. Then, in order to reduce local over saturation of HPMSM, the stator slot is improved under the condition of the same outer dimension. The simulation and experiment results are done to verify the design and optimization method. It is found that the improved HPMSM can increase the output torque largely and reduce the torque ripple effectively.

References

[1] D. Hong, W. Hwang, J. Lee and B. Woo, "Design, Analysis, and Experimental Validation of a Permanent Magnet Synchronous Motor for Articulated Robot Applications," *IEEE Transactions on Magnetics*, vol. 54, no. 3, pp. 1-4, 2017.

[2] K. Lee, J. Lee, B. Woo, J. Lee, Y. Lee and S. Ra, "Modeling and Control of a Articulated Robot Arm with Embedded Joint Actuators," in *Proc. of 2018 International Conference on Information and Communication Technology Robotics (ICT-ROBOT)*, Busan, pp. 1-4, 2018.

[3] K. Lee et al., "High precision hand-eye self-calibration for industrial robots," in *Proc. of 2018 International Conference on Electronics, Information, and Communication (ICEIC)*, Honolulu, HI, pp. 1-5, 2018.

[4] A. De et al., "Task-Based Control and Design of a BLDC Actuator for Robotics," *IEEE Robotics and Automation Letters*, vol. 4, no. 3, pp. 2393-2400, 2019.

[5] W. Zhang et al., "Electromagnetic design of a high torque density permanent magnet motor for biomimetic robot," in *Proc. of 2017 IEEE International Conference on Cyborg and Bionic Systems (CBS)*, Beijing, pp. 140-144, 2017.

[6] F. Kung, "Design of agile two-wheeled robot with machine vision," in *2017 International Conference on Robotics, Automation and Sciences (ICORAS)*, Melaka, 2017, pp. 1-5.

[7] J. Kwon et al., "Development of flux switching PM machines with phase-group concentrated-coil windings for robot applications," in *Proc. of 2016 IEEE Conference on Electromagnetic Field Computation (CEFC)*, Miami, FL, pp. 1-4, 2016.

[8] J. Seo, et al., "Design of axial flux permanent magnet brushless DC motor for robot joint module, " in *Proc. of 2010 International Power Electronics Conference - ECCE ASIA, Sapporo*, pp. 1336-1340, 2010.

[9] H. Yin, Y. Yu and J. Li, "Optimization design of a motor embedded in a lightweight robotic joint," in *Proc. of 2017 12th IEEE Conference on Industrial Electronics and Applications (ICIEA)*, Siem Reap, pp. 1630-1634, 2017.

[10] W. Zhang et al., "Electromagnetic design of a high torque density permanent magnet motor for biomimetic robot," in *Proc. of 2017 IEEE International Conference on Cyborg and Bionic Systems (CBS)*, Beijing , pp. 140-144, 2017

[11] K. Halbach. "Design of permanent multipole magnets with oriented rare earth cobalt materials," *Nuclear Instruments and Methods*, vol. 169, no. 1, pp. 1-10, 1980.

[12] K. Halbach. "Permanent magnets for Production and use of high energy beams," in *Proceedings of the 8th International Workshop on Rare-earth Permanent Magnets*, pp. 123-136, 1985.

[13] X. Zhang, C. Zhang, J. Yu, P. Du and L. Li, "Analytical Model of Magnetic Field of a Permanent Magnet Synchronous Motor With a Trapezoidal Halbach Permanent Magnet Array," *IEEE Transactions on Magnetics*, vol. 55, no. 7, pp. 1-5, 2019.

[14] Y. Guo et al., "Improved Fuzzy-Based Taguchi Method for Multi-Objective Optimization of Direct-Drive Permanent Magnet Synchronous Motors," *IEEE Transactions on Magnetics*, vol. 55, no. 6, pp. 1-4, 2019.

[15] C. T. Krasopoulos et al., "Hybrid multi-objective optimization algorithm for PM motor design," in *Proc. of 2016 IEEE Conference on Electromagnetic Field Computation (CEFC)*, Miami, FL, pp. 1-5, 2016.

[16] X. Cao et al., "Multi-objective optimization of permanent magnet synchronous motor based on elite retention hybrid simulated annealing algorithm," in *Proc. of 2017 12th IEEE Conference on Industrial Electronics and Applications (ICIEA)*, Siem Reap, pp. 535-540, 2017.

[17] Behrooz Rezaeealam, Farhad Rezaee-Alam, "A new optimal design of surface mounted permanent magnet synchronous motors with integral slot per pole", *COMPEL - The international journal for computation and mathematics in electrical and electronic engineering*, vol. 37 Issue: 1, pp.136-152, 2018.

[18] H. Wang, Y. Du, L. Shi, R. Zhang and Q. Ge, "The Multi-Objective Optimization of Ironless Permanent Magnet Linear Synchronous Machine with Unequal Halbach Array," in *Proc. of 2019 12th International Symposium on Linear Drives for Industry Applications (LDIA)*, Neuchatel, Switzerland, pp. 1-4, 2019.

[19] Z. Wen, B. Xiong and G. Gu, "Optimization Design of Low Speed Axial Flux Halbach Permanent-Magnet Generator with PCB Winding," in *Proc. of 2019 22nd International Conference on Electrical Machines and Systems (ICEMS)*, Harbin, China, pp. 1-4, 2019.

[20] L. Yang, S. L. Ho and W. Fu, "Design optimization of a permanent magnet motor with a modified Halbach magnetization," in *2015 IEEE International Magnetics Conference (INTERMAG)*, Beijing, pp. 1-5, 2015.

Shuangshuang Zhang was born in Yancheng, Jiangsu, China in 1995. She received the B. Sc. degree in electrical engineering from Zhonghuan Information College Tianjin University of Technology, Tianjin, China, in 2018, and currently working toward the M. Sc. degree in Control Science and Engineering in Nantong University, Nantong, China. Her current research interest in design and optimization of halbach motors.

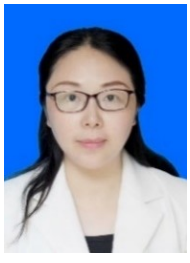

Wei Zhang was born in Taizhou, Jiangsu, China in 1977. She received the B. Sc. degree in electrical engineering from Nantong University, Nantong, China, in 2000, and the M. Sc. degree and the Ph. D. degree in electrical engineering from Southeast University, Nanjing, China, in 2007 and in 2016, respectively. Since 2000, she has been with Nantong University where she is a professor in the college of electrical engineering. From January 2017 to December 2017, she was a visiting scholar at the University of Sheffield, Sheffield, UK. Her current major research interests include design and control of permanent magnet brushless machines and drives for automotive applications, and renewable energy applications.

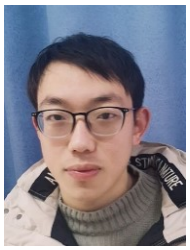

Rui Wang was born in Huaian, Jiangsu, China in 1997. He received the B. Sc. degree in electrical engineering and Intelligent Control from Nantong University, Nantong, China, in 2019, and currently working toward the M. Sc. degree in Control Science and Engineering in Nantong University, Nantong, China. His current research interest is design and optimization of axial field flux-switching permanent magnet machine.

Xu Zhang was born in Suqian, Jiangsu, China in 1993. He received the B.Sc. degree in electrical engineering from Jincheng College of Nanjing University of Aeronautics and Astronautics, China, in 2017, and currently working toward the M. Sc. degree in Control Science and Engineering in Nantong University, Nantong, China. His current major research interest is electromagnetic design and multi-objective optimization of axial field flux switching permanent magnet machine.

Xiaotong Zhang was born in Taiyuan, Shanxi, China in 1997. Since 2016, she studied at Nantong University and is currently a student of the School of Electrical Engineering. Her current research interests include the design and control of permanent magnet motors.